The Tropical–Extratropical Interaction between High-Frequency Transients and the Madden–Julian Oscillation

ADRIAN J. MATTHEWS*

Cooperative Institute for Research in Environmental Sciences, University of Colorado/NOAA, Boulder, Colorado

GEORGE N. KILADIS

NOAA Aeronomy Laboratory, Boulder, Colorado

(Manuscript received 24 July 1997, in final form 20 April 1998)

ABSTRACT

The interaction between high-frequency transient disturbances and convection, and the Madden–Julian Oscillation (MJO), is investigated using NCEP–NCAR reanalysis and satellite outgoing longwave radiation data for 15 northern winters. During the phase of the MJO with enhanced convection over the East Indian Ocean and Indonesia, and suppressed convection over the South Pacific convergence zone, both the Asian–Pacific jet and the region of upper-tropospheric tropical easterlies over the warm pool are displaced westward. These changes in the basic state lead to a weaker or ''leakier'' waveguide in the Asian–Pacific jet, with a westward-displaced ''forbidden'' region of tropical easterlies, such that high-frequency transient waves propagate equatorward into the deep Tropics over the central Pacific near the date line. As these waves induce convection in the region of ascent and reduced static stability ahead of the upper-level cyclonic disturbances, there is an enhancement of high-frequency convective variability over the central Pacific intertropical convergence zone during this phase of the MJO. This enhanced high-frequency convective variability appears to project back onto intraseasonal timescales and forms an integral part of the slowly varying diabatic heating field of the MJO. In the opposite phase of the MJO, the Asian–Pacific jet is extended eastward and there is an almost continuous waveguide across the Pacific. Together with the expanded forbidden region of tropical easterlies over the warm pool, this leads to a more zonal propagation of high-frequency transients along the waveguide with less equatorward propagation, and hence reduced high-frequency convective variability over the tropical central Pacific. There is also evidence of high-frequency waves propagating into the Indian Ocean region at the beginning of the MJO cycle, which may be important in the initiation of intraseasonal convective anomalies there.

1. Introduction

In the central and eastern Pacific in northern winter and spring, deep convection along the intertropical convergence zone (ITCZ) is observed to occur preferentially in conjunction with the equatorward propagation of extratropical wave trains from the Northern Hemisphere (Liebmann and Hartmann 1984; Kiladis and Weickmann 1992a,b). The convection occurs ahead of an upper-level trough or positive potential vorticity (PV) anomaly in the wave train, in the region of ascent and reduced static stability (Kiladis 1998). Lagged regression relationships show that the propagation of the wave train into the Tropics precedes the development of the ITCZ convection, inferring that the convection is induced by the wave dynamics. Even though the circulation and PV anomaly of the waves is a maximum in the upper troposphere, it still induces ascent throughout the whole troposphere down to the boundary layer (Matthews et al. 1996). Subsequently, a southwest–northeast-oriented cloud band frequently develops from the convection over the ITCZ. The wave trains have a mean period of about 12 days and therefore occur at a lower frequency than typical midlatitude baroclinic eddies, but at a higher frequency than the dominant mode of intraseasonal variability over the Pacific—the Madden–Julian Oscillation [MJO, see Madden and Julian (1994) for a review].

The equatorward-propagating waves, hereafter referred to as ''wave activity,'' and the associated convection are an essential part of the general circulation of the eastern Pacific region. The waves have a positive southwest–northeast tilt and transport westerly momentum poleward. This momentum transport is a significant part of the momentum budget in the region (Kiladis and

* Current affiliation: CRC for Southern Hemisphere Meteorology, Monash University, Clayton, Victoria, Australia.

Corresponding author address: Dr. Adrian J. Matthews, CRC for Southern Hemisphere Meteorology, Monash University, 3rd Floor, Bldg. 70, Wellington Rd., Clayton, Victoria 3168, Australia.
E-mail: ajm@vortex.shm.monash.edu.au

Feldstein 1994). Climatological rainfall rates over the eastern Pacific ITCZ in the northern winter are very high, estimated to be of the order of 10 mm day^{-1} (Janowiak et al. 1995), corresponding to a latent heating of 300 W m^{-2}, or 2.5°C day^{-1}. The response to such a heat source includes an extratropical wave train over the Pacific and North America (Jin and Hoskins 1995).

The wave activity in the region of equatorial westerlies in the eastern Pacific can be explained by the Rossby wave theory using ray tracing (Hoskins and Ambrizzi 1993) and shallow water calculations (Webster and Holton 1982) on a time-mean flow that varies in longitude as well as latitude. The tropical easterlies in the upper troposphere over the Eastern Hemisphere act as a barrier to Rossby wave propagation into the Tropics, producing a ''critical line'' for Rossby waves whose zonal phase speed approaches that of the background flow (e.g., Yang and Hoskins 1996). However, in northern winter, there are mean upper-tropospheric westerlies on the equator over the eastern Pacific and the Atlantic. These mean westerlies allow Rossby waves to propagate into the deep Tropics in these regions and even to cross the equator. As the waves propagate from the midlatitudes into the Tropics, their vertical scale shrinks (Kiladis 1998) and they are confined to the region of westerlies in the upper troposphere; the mean easterlies in the tropical lower troposphere preclude barotropic Rossby wave propagation there (Tomas and Webster 1994).

Ray tracing and refractive index arguments predict that the subtropical jets will act as waveguides (Hoskins and Ambrizzi 1993). The theory suggests that, upon exiting the particularly strong waveguide of the Asian–Pacific jet, a wave train may split into two parts—one continuing over North America, and the other being refracted southward into the equatorial westerlies over the eastern Pacific, in agreement with observations (Kiladis and Weickmann 1992b; Kiladis 1998).

Previous observational and ray-tracing work described above indicates that the Asian jet is a source region for these wave trains. One possible excitation mechanism is transient convection over the Indian Ocean. This appears to force a wave train in the jet of similar zonal wavenumber (5–6) to the waves observed in the eastern Pacific (Meehl et al. 1996; Kiladis and Weickmann 1997). Alternatively, midlatitude baroclinic waves have been observed to travel around the globe at the latitude of the jet in groups or wave packets (Lee and Held 1993; Chang 1993). The period of the envelope of wave activity is around 10 days, which is similar to that of the waves observed over the tropical eastern Pacific (Kiladis 1998).

It is clear that the slowly evolving, large-scale background flow, or ''basic state'' is crucial to the propagation characteristics of the eastern Pacific wave trains. Hence, low-frequency changes in the basic state may lead to different propagation characteristics and subsequently to changes in the convection and the transient circulation of the region. The largest changes to the basic state occur as part of the annual cycle. In northern summer and fall, the upper-tropospheric equatorial westerlies over the eastern Pacific are replaced by easterlies over almost the whole tropical domain. These easterlies preclude the propagation of Rossby wave activity into the eastern Pacific, and there is no connection between extratropical wave trains and convection over the ITCZ in northern summer and fall (Kiladis and Weickmann 1997).

The basic state also changes on interannual timescales, mainly as a result of El Niño–Southern Oscillation. For example, the winter of 1982–83 was a strong warm event, and the main area of convection was situated over the central Pacific, eastward of its mean position. The node between the equatorial easterlies and westerlies was also shifted eastward, to 130°W, and the strength of the westerly ''duct'' in the equatorial eastern Pacific was much reduced. Consequently, much less wave activity propagated into the tropical central Pacific (Kiladis 1998), and the occurrence of cloud bands was reduced (McGuirk et al. 1987). In contrast, the winter of 1988–89 was characterized by cold event conditions. The westerly duct was stronger than usual, and wave activity and cloud band occurrence in the eastern Pacific were enhanced. Over the Atlantic, the situation is reversed, with stronger equatorial westerlies during a warm event. The barotropic model calculations of Ambrizzi (1994) predict greater cross-equatorial propagation over the Atlantic during such a warm event.

On intraseasonal timescales, the MJO involves an eastward translation of tropical convective anomalies from the Indian Ocean to the western Pacific, and subsequently to South America and Africa, with a period of between 30 and 60 days. The convective anomalies have associated wind and mass perturbations, including significant anomalies in the region of the tropical eastern Pacific (Knutson and Weickmann 1987). Previous work on the interaction between high-frequency transients and the MJO has focused on the warm pool region. Super cloud clusters (SCCs) with horizontal scales of several thousand kilometers propagate slowly eastward and can be identified as MJO convective anomalies. Within the envelope of these SCCs, cloud clusters with scales of hundreds of kilometers propagate westward in the opposite direction (Nakazawa 1988; Lau et al. 1991). Synoptic and mesoscale activity is also enhanced during this convectively active phase of the MJO (Hendon and Liebmann 1994; Weng and Lau 1994). In particular, there is a westward-propagating mode with a period of approximately 2 days (Hendon and Liebmann 1994; Chen et al. 1996; Chen and Houze 1997), which can be identified with $n = 1$ westward-propagating inertio-gravity waves (Takayabu 1994). The diurnal cycle over the maritime continent is also strongly modulated by the MJO, although in an inverse sense. During the convectively active (inactive) phase of the MJO, the diurnal cycle is suppressed (enhanced) (Sui and Lau 1992).

High-frequency transients may have a role to play in

the initiation of the convectively active phase of the MJO over the Indian Ocean. In a case study of an MJO in the northern winter of 1985–86, Hsu et al. (1990) found that convection in the Indian Ocean became organized only when a subtropical Rossby wave train propagated into the region. The convection was initially located in the ascent region ahead of a trough in the wave train and then developed into an MJO. In an idealized modeling study, Bladé and Hartmann (1993) found that baroclinic waves propagating into the Tropics from the Asian jet could force ascent and deep convection in the subtropics ahead of a trough. Once again, this deep convection then evolved into an MJO.

However, the interaction between high-frequency transients and the MJO in the central and eastern Pacific region appears to have been neglected. The aim of this paper is to investigate the interaction between high-frequency wave activity and transient convection, and the MJO, with particular emphasis on the eastern Pacific ITCZ region, and to attempt to relate these interactions to changes in the basic state during the MJO life cycle.

2. Data and methodology

a. Data

Data from 15 northern winters (December–February, DJF) from 1979–80 to 1993–94, were used in this study. Daily mean winds at 200 mb were obtained from the National Centers for Environmental Prediction–National Center for Atmospheric Research (NCEP–NCAR) reanalysis dataset (Kalnay et al. 1996). The reanalysis uses the same state-of-the-art data assimilation scheme throughout the whole period and therefore provides a consistent dataset free of the problems caused by changes to the assimilation scheme in the operational analyses. Outgoing longwave radiation (OLR) data from the National Oceanic and Atmospheric Administration (NOAA) satellites (Liebmann and Smith 1996) were used as a proxy for tropical convection (Arkin and Ardanuy 1989). Both datasets are stored on the same 2.5° latitude × 2.5° longitude grid.

b. Lagged regression technique

To show the evolution of the slowly evolving basic state, and the behavior of the high-frequency transients throughout the MJO, lagged regression techniques were employed, similar to those in Kiladis and Weickmann (1992a). A time series was constructed from daily values of an area-averaged OLR over a 20° × 20° box in the western Pacific warm pool (15°S–5°N, 140°–160°E). The daily OLR time series was passed through a 30–70-day bandpass Lanczos filter (Duchon 1979) with 241 weights to isolate the MJO signal. This is then the ''warm pool OLR'' reference time series against which other variables were regressed. The regression maps, shown later, are scaled to a value of -20 W m^{-2} of the reference time series, a typical minimum value during the passage of an MJO through the region.

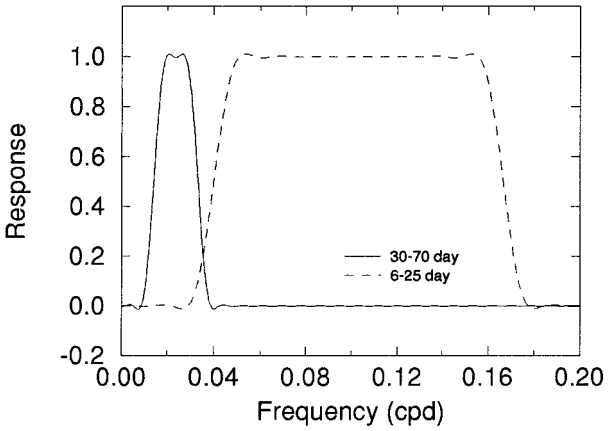

FIG. 1. Filter response curves for 30–70-day (solid) and 6–25-day (dashed) bandpass filters.

The gridded fields of daily mean 200-mb wind and OLR were passed through the same 30–70-day filter and regressed against the reference time series. The slowly evolving wind field anomalies, when added back to the climatological mean, may be used to describe the basic state on which the high-frequency transients propagate, and the OLR anomalies describe the slowly evolving convective envelope of the ''typical'' MJO. However, for reasons outlined later, a compositing procedure, rather than the regression technique described here, is used to reconstruct the basic state at different phases of the MJO.

To isolate the high-frequency transients, the gridded fields of daily mean 200-mb winds and OLR were passed through a 6–25-day bandpass filter. The 6-day low-pass cutoff was chosen to exclude higher frequency baroclinic waves, and the 25-day high-pass cutoff, rather than the 30-day high-pass cutoff used in the earlier studies of Kiladis and Weickmann, was chosen to clearly separate the high-frequency transients from the 30–70-day filtered MJO signal. As seen in Fig. 1, there is very little overlap between the response curves of the two filters. The terms ''high frequency'' and ''6–25-day filtered'' will be used interchangeably from here.

As they are from different frequency bands, a simple regression of the 6–25-day filtered wind fields against the 30–70-day filtered reference time series would only yield noise with near-zero correlation. An exact relationship between the phase of the high-frequency transients and the phase of the slowly evolving MJO would not be expected in any case. Instead, an enhancement of convection and wave activity on the 6–25-day timescale in a certain phase of the MJO was anticipated. Hence, the variance of the 6–25-day filtered OLR fields was regressed against the reference time series. Before the regression, the squared 6–25-day filtered OLR fields were passed through the 30–70-day filter to isolate that

portion of the variance that fluctuates on MJO timescales. The regression calculation of the high-frequency squared OLR perturbations, and of other high-frequency quadratic quantities described below, is analogous to a weighted time average, where the reference time series acts as a weighting function. A similar measure of the ''variance'' of the high-frequency waves is the perturbation kinetic energy (PKE):

$$\text{PKE} = \frac{1}{2}(\overline{u'^2 + v'^2}), \tag{1}$$

where u' and v' are the 6–25-day filtered zonal and meridional wind, respectively. Daily maps of PKE were then passed through the 30–70-day filter and regressed against the reference time series.

Another second-order quantity that can be calculated from the 6–25-day-filtered wind field is the ''E vector'' (Hoskins et al. 1983):

$$\mathbf{E} = (\overline{v'^2 - u'^2}, -\overline{u'v'}). \tag{2}$$

The E vectors give information about the shape and propagation characteristics of eddies and their feedback onto the mean flow and are approximately parallel to the group velocity of the waves. Daily maps of both components of the E vector were passed through the 30–70-day filter and regressed against the reference time series. The lagged regression maps thus produced show how the high-frequency E vectors, and the propagation characteristics of the high-frequency eddies they describe, change over the MJO life cycle.

c. Statistical significance

To ensure that the results of the lagged regression analysis were not due merely to chance, a statistical significance test was performed following Livezey and Chen (1983; hereafter LC). First, the local statistical significance at each grid point of the regression map was determined. As both the reference time series and the gridpoint fields showed considerable temporal autocorrelation, each day of data was not independent. Hence, a decorrelation timescale for each gridpoint was calculated [see Eq. (1) of LC]. The number of temporal degrees of freedom was then calculated from the decorrelation timescale before assessing local significance at the 95% level.

If each grid point was independent and the dataset was of infinite length, then even if there was no deterministic relationship between the reference time series and the gridpoint fields, 5% of the grid points (weighted by area) would be expected to be locally significant at the 95% level purely by chance. However, due to the existence of spatial correlations between neighboring grid points and the finite length of the data, considerably more than 5% of the area of the globe could appear to be locally significant at the 95% level—still purely by chance.

Therefore, to determine the ''global significance'' of the regression fields, 1000 Monte Carlo simulations were performed for each variable. In each simulation, a reference time series was generated randomly from a Gaussian distribution and the daily gridpoint fields were regressed against it. For each simulation, the percentage of area locally significant at the 95% level was calculated and used to build up a histogram giving a frequency distribution of the percentage of locally significant area. These frequency distributions were centered near 5% but had considerable spread about this mean value. If the actual percentage of area significant at the 95% level from the original regression was greater than, say, the 99th percentile of the histogram, then the regression field was said to be globally significant at this level (99%). If this criterion was not met, then the seemingly large area of local significance could have just arisen by chance, and any physical arguments drawn from the regression analysis must be treated with caution.

d. Compositing technique

In section 2b, reconstruction of the slowly evolving basic state (the MJO), upon which the high-frequency transients propagate, was described. This was accomplished by adding back the 30–70-day wind anomalies to the climatological mean. However, the initial scaling of these wind anomalies (i.e, the chosen reference OLR value of -20 W m^{-2}) was rather arbitrary. As one of the diagnostics to be calculated from the basic state, the total stationary wavenumber (Hoskins and Ambrizzi 1993), is highly nonlinear and, therefore, sensitive to this scaling, an alternative approach is preferred.

In this approach, a composite-mean basic state was constructed using the 30–70-day filtered warm pool OLR reference time series of the regression analyses. A day on which this reference time series was a minimum and less than one standard deviation was denoted as a ''day 0.'' There were 23 such day 0s from DJF 1979–80 to 1993–94—that is, 23 individual MJO events. To calculate the composite-mean basic state appropriate to, say, day -10 of the MJO life cycle, the daily mean 200-mb zonal wind fields from day -15 to day -5 of each of the 23 individual MJO events were averaged. The 11 days from day -15 to day -5 of each MJO constitute approximately a quarter cycle of the MJO, which is about the longest period over which the slowly varying flow field of the MJO can be assumed to remain roughly constant—that is, over which it can be considered a background basic state. The resulting composite-mean 200-mb zonal wind field was then denoted the ''day -10 phase.'' Similarly, the ''day $+10$ phase'' was constructed by averaging over the 253 (11×23) daily mean fields from day $+5$ to day $+15$ of the 23 individual MJO events.

The composite mean OLR field for the day 0 phase (day -5 to day $+5$) was also calculated and compared with the mean DJF OLR field. The anomaly in the com-

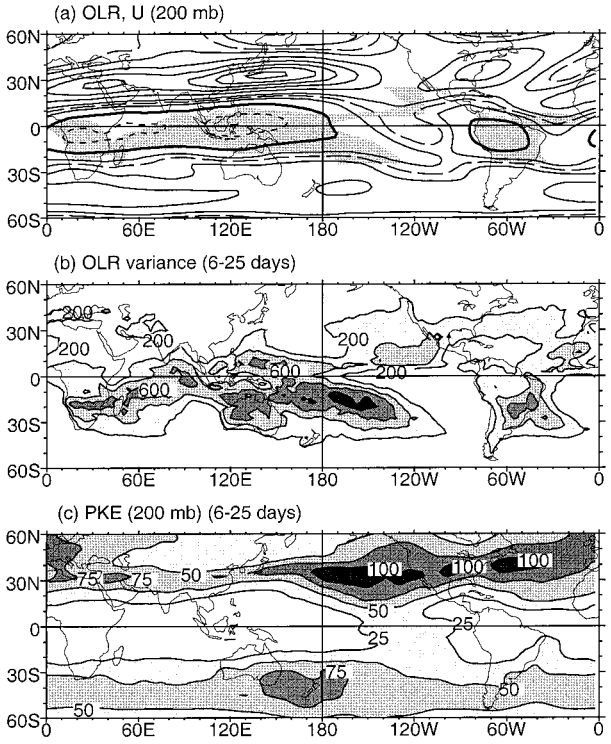

FIG. 2. Mean fields for DJF from 1979–80 to 1993–94. (a) OLR and 200-mb zonal wind. OLR values less than 245 W m^{-2} are shaded from 25°S to 25°N only. Contour interval for 200-mb zonal wind is 10 m s^{-1}. Positive (negative) contours are solid (dashed), the zero contour is thickened, and an extra contour at 15 m s^{-1} is long-dashed. (b) High-frequency (6–25 day) OLR variance. Contour interval is 200 W^2 m^{-4}, and values above 200 W^2 m^{-4} are shaded. (c) High-frequency (6–25 day) 200-mb PKE. Contour interval is 25 m^2 s^{-2}, and values above 25 m^2 s^{-2} are shaded.

posite mean OLR field for the day 0 phase over the 20° × 20° box (15°S–5°N, 140°–160°E) was very close to −20 W m^{-2}, indicating the suitability of the chosen reference value of −20 W m^{-2} used in the regression analysis.

3. Climatological mean basic state

To help interpret the results of the regression analysis, some northern winter mean fields are first discussed. The mean 200-mb zonal wind (Fig. 2a) is dominated by the subtropical jets over the Northern Hemisphere. In particular, the Asian–Pacific jet maximum is over 70 m s^{-1}, southeast of Japan. Easterlies cover most of the equatorial region, except for the ''westerly ducts'' over the central and eastern Pacific, and the Atlantic. Note especially the local equatorial maximum in zonal wind, outlined by the extra, long-dashed 15 m s^{-1} contour in the eastern Pacific. The mean OLR in Fig. 2a shows the regions of deep tropical convection over Africa, the warm pool, and the South Pacific convergence zone (SPCZ), the Amazon Basin, and along the zonally oriented ITCZ at about 8°N over the central and eastern Pacific.

The lower two panels of Fig. 2 show diagnostics of the high-frequency (6–25 day) transients. The pattern of variance of OLR on the 6–25-day timescale (Fig. 2b) roughly follows that of the mean low OLR (Fig. 2a); that is, the regions of high-frequency convective variability coincide with the regions of mean convection. However, there is a local minimum in the high-frequency convective variability over the islands of the equatorial warm pool, even though the mean convection there is strong. Spectral decomposition of the OLR variance over these islands indicates that the diurnal cycle is the dominant mode of variability (Salby et al. 1991). Regions of frequent cloud band activity are also seen as northeastward extensions of variance in the eastern Pacific and eastern Atlantic.

To indicate the preferred locations of high-frequency transient activity, 200-mb PKE on the 6–25-day timescale is shown in Fig. 2c. The largest values, over 100 m^2 s^{-2}, are found in the subtropics, particularly in the jet exit regions over the North Pacific and the North Atlantic. The areas of tropical easterlies are relatively quiescent, with mean PKE less than 25 m^2 s^{-2}, but the higher values in the westerly ducts over the Pacific and, to a lesser extent, the Atlantic, reflect the existence of wave activity in these regions (see Arkin and Webster 1985).

The stationary wavenumber of the 200-mb mean zonal flow is shown in Fig. 3 [see Hoskins and Ambrizzi (1993) for a discussion] with mean high-frequency E vectors, on the 6–25-day timescale, superimposed. Total stationary wavenumber is defined as

$$K_s = \left(\frac{\beta - \overline{U}_{yy}}{\overline{U}}\right)^{1/2}, \tag{3}$$

where $\overline{U}$ is the time-mean zonal wind, β is the meridional planetary vorticity gradient, and $-\overline{U}_{yy}$ is the time-mean meridional relative vorticity gradient (the contribution from the meridional wind has been neglected). The term K_s acts as a refractive index for stationary Rossby waves, such that waves are refracted toward (away from) regions of high (low) K_s. The regions of mean easterlies correspond to imaginary values of the stationary wavenumber (darkest shading). The boundaries of these regions are demarcated by a critical, or zero wind, line toward which Rossby waves are refracted. The critical line may then act as an absorber or reflector of Rossby waves (Killworth and McIntyre 1985). However, once inside the region of imaginary stationary wavenumber, the Rossby waves become evanescent and decay rapidly. Consistent with theory, the amplitude of the E vectors and the PKE magnitudes (Fig. 2c) are very small in these regions. Although the 6–25-day waves are clearly not stationary, a similar total wavenumber for the transient waves can be calculated (Yang and Hoskins 1996). Following Kiladis (1998), K_s is used here to give a

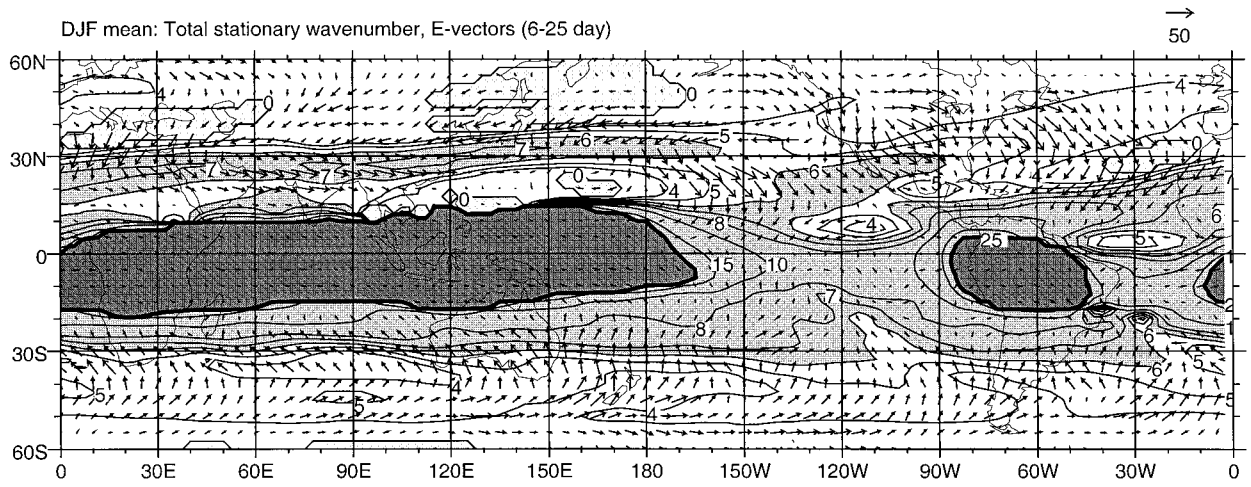

FIG. 3. Mean fields for DJF from 1979–80 to 1993–94. The 200-mb total stationary wavenumber K_s is contoured at zonal wavenumbers 0, 4, 5, 6, 7, 8, 10, 15 with a thickened contour at 25 to represent the transition to regions of easterly zonal wind and imaginary K_s. Regions of negative absolute vorticity gradient are shaded lightly; regions between zonal wavenumbers 6–25 and of easterly zonal wind are shaded with increasing darkness. Also shown are high-frequency (6–25 day) 200-mb E vectors. Reference vector is 50 $m^2 s^{-2}$.

qualitative description of the effects of the basic state on the propagation of the transient waves.

The waveguide nature of the subtropical jets can be seen from the axes of maximum stationary wavenumber that lie along the jet axes, especially in the Asian–Pacific jet. The E vectors tend to point in an approximately zonal direction along the Asian jet core, indicating the tendency for 6–25-day Rossby wave energy to propagate along the jet. However, there is also a significant cross-jet component of the E vectors, indicating the ''leaky'' nature of the waveguide. In the region of the Asian–Pacific jet exit, the E vectors point southeastward toward the equatorial central Pacific and the higher values of stationary wavenumber. These southeastward-pointing E vectors extend across the equator into the Southern Hemisphere to 5°S, near 110°W, indicating cross-equatorial propagation. Southern Hemisphere waves are also refracted equatorward toward the westerly duct, as shown by the northward-pointing E vectors in a region centered on 15°S, 150°W.

Over the ITCZ in the eastern Pacific at 8°N, 110°W, there is a local minimum in stationary wavenumber. This arises from a weakening of the meridional vorticity gradient due to a minimum in the zonal wind between the equatorial westerly maximum to the south and the North American jet to the north (Fig. 2a). As indicated by the E vectors, Rossby waves will be refracted away from this region, even though the strongest equatorial westerlies are found at this longitude.

4. Slowly evolving basic state of the MJO

The slow evolution of the basic state over an MJO life cycle is shown (in Fig. 4) by lagged regression maps of 30–70-day filtered 200-mb zonal wind and OLR, regressed against the warm pool OLR reference time series. This brief section is intended as a framework to put the behavior of the high-frequency transient anomalies in context. Results are similar to those of Knutson and Weickmann (1987) and Hendon and Salby (1994), for example. Individual MJOs may differ significantly from the mean life cycle described here. This point is discussed further in section 7.

On day −10 (Fig. 4a) there is enhanced convection over the warm pool and Australia, with reduced convection over the date line and the SPCZ. The equatorial 200-mb zonal wind anomalies are westerly over the western and central Pacific, and easterly from the eastern Pacific eastward to the Indian Ocean. The Asian–Pacific jet is retracted over the Pacific, with subtropical easterly anomalies up to −6 m s^{-1} over the Pacific (30°N, 180°). The jet entrance region over Asia is strengthened with westerly anomalies of up to 4 m s^{-1}.

Ten days later, on day 0 (Fig. 4b), the MJO convection has moved eastward to be centered over the western Pacific, and convection over Brazil, Africa, and the Indian Ocean is suppressed. Equatorial 200-mb westerly anomalies have expanded rapidly eastward from the central Pacific to North Africa, and the Asian–Pacific jet is now strengthened, with peak westerly anomalies at 35°N.

By day +10 (Fig. 4c), the enhanced convection of the MJO has moved farther eastward to the date line and the SPCZ, while convection over the whole Indian Ocean and Maritime Continent is suppressed. There are easterly anomalies over the tropical western and central Pacific and westerly anomalies over the rest of the Tropics. The Asian–Pacific jet has positive anomalies over the western and central Pacific out to 150°W. This phase of the MJO is approximately opposite to that at day −10.

On day +20 (Fig. 4d) there is a large region of sup-

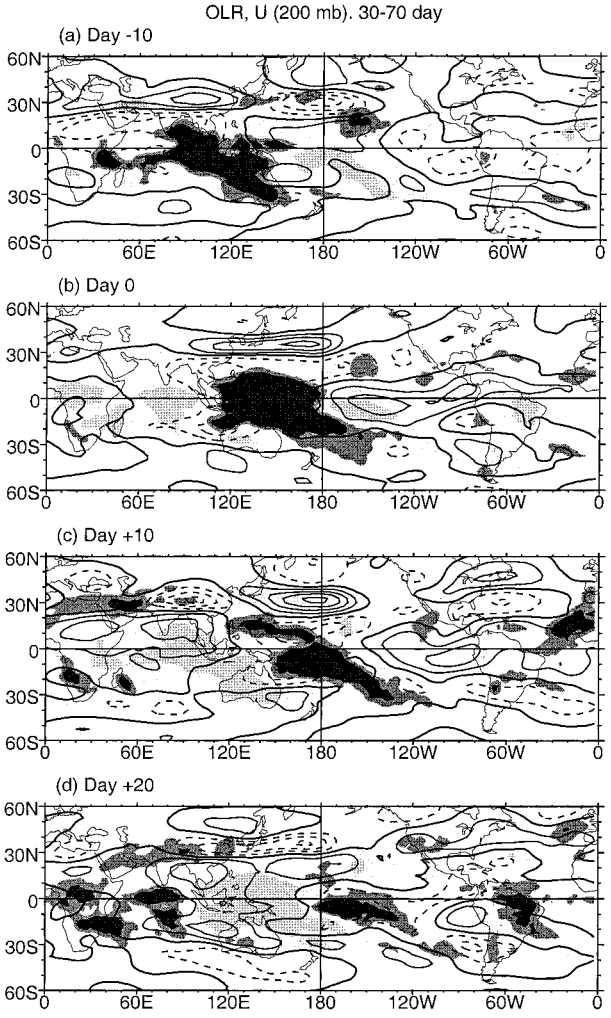

FIG. 4. Lagged regression maps of 30–70-day filtered OLR and 200-mb zonal wind for an OLR anomaly of −20 W m^{-2} over the region (15°S–5°N, 140°–160°E). OLR is shaded darkly below −6 and −3 W m^{-2}, and lightly above +3 and +6 W m^{-2}. The 200-mb zonal wind contour interval is 2 m s^{-1}. Positive (negative) contours are solid (dashed), and the zero contour is thickened. (a) day −10, (b) day 0, (c) day +10, and (d) day +20.

pressed convection over the warm pool, and the enhanced convection of the next MJO is beginning over the Indian Ocean. The Asian–Pacific jet is now at its weakest with negative zonal wind anomalies at 30°N. The anomalies at day +30 (not shown) are similar to those at day −10, hence one cycle of the MJO has been completed in approximately 40 days.

All the anomalies described in this section are locally statistically significant at the 95% level. The results of the Monte Carlo global significance tests are summarized in Table 1. This shows the percentage of area that is locally significant at the 95% level for both 30–70-day filtered OLR and 200-mb zonal wind for the lags shown in Fig. 4. Note that all the regression maps are globally significant at (well above) the 99% level.

TABLE 1. Field significance of regression maps shown in Fig. 4. The percentage of area that is locally statistically significant at the 95% level is shown for 30–70-day filtered OLR and 200-mb zonal wind regressed against the 30–70-day filtered reference OLR time series at various lags. All fields are globally significant at the 99% level.

Day	OLR	*U* (200 mb)
−10	21.4	30.7
0	23.6	24.6
+10	25.5	36.9
+20	23.5	25.5

5. Interaction between high-frequency transients and the MJO

Figures 5, 6, and 7 show the lagged regression maps of the high-frequency (6–25 day) 200-mb PKE, 200-mb E vectors, and OLR variance anomalies for days −10, +10, and +20 of the MJO life cycle, respectively. The local and global significance of the regression maps of the high-frequency transients are summarized in Table 2. On day −10, the regression maps of PKE and OLR variance are highly globally significant at greater than the 99% level. The regression map of E vectors is also globally significant, at the 90% and 95% level, for the *x* and *y* components, respectively. On day 0, the 30–70-day zonal wind anomalies (Fig. 4b), although still large, are such that when the basic state is reconstructed for this phase of the MJO, there is little change in the stationary wavenumber field from the climatological mean (Fig. 3). Hence, there is little change in the propagation characteristics of the high-frequency waves, and the regression map of E vectors is not globally significant at the 90% level. For days +10 and +20, all regression maps are globally significant, at greater than the 95% significance level.

a. Warm pool sector

The relationship between high-frequency transients and the MJO envelope over the warm pool sector, from the Indian Ocean to the western Pacific, is described in this section. On day −10 there is enhanced convection on the 30–70-day timescale over the warm pool (Fig. 4a). However, over the equatorial islands of the warm pool, especially Borneo and New Guinea, there are only weak MJO convective anomalies, which is consistent with previous studies of the MJO. The enhanced 30–70-day warm pool convection coincides with enhanced off-equatorial (i.e., along the margins of the envelope) high-frequency convective variability (Fig. 5c) in both hemispheres from around 80°E to 135°E. On the equator itself, in the region of the local minimum in the mean high-frequency OLR variance described in section 3, the anomalies in high-frequency convective variability are near zero or slightly negative. The largest increase in variance is over the Bay of Bengal. In this region, the local correlation coefficient exceeds 0.4; hence, up

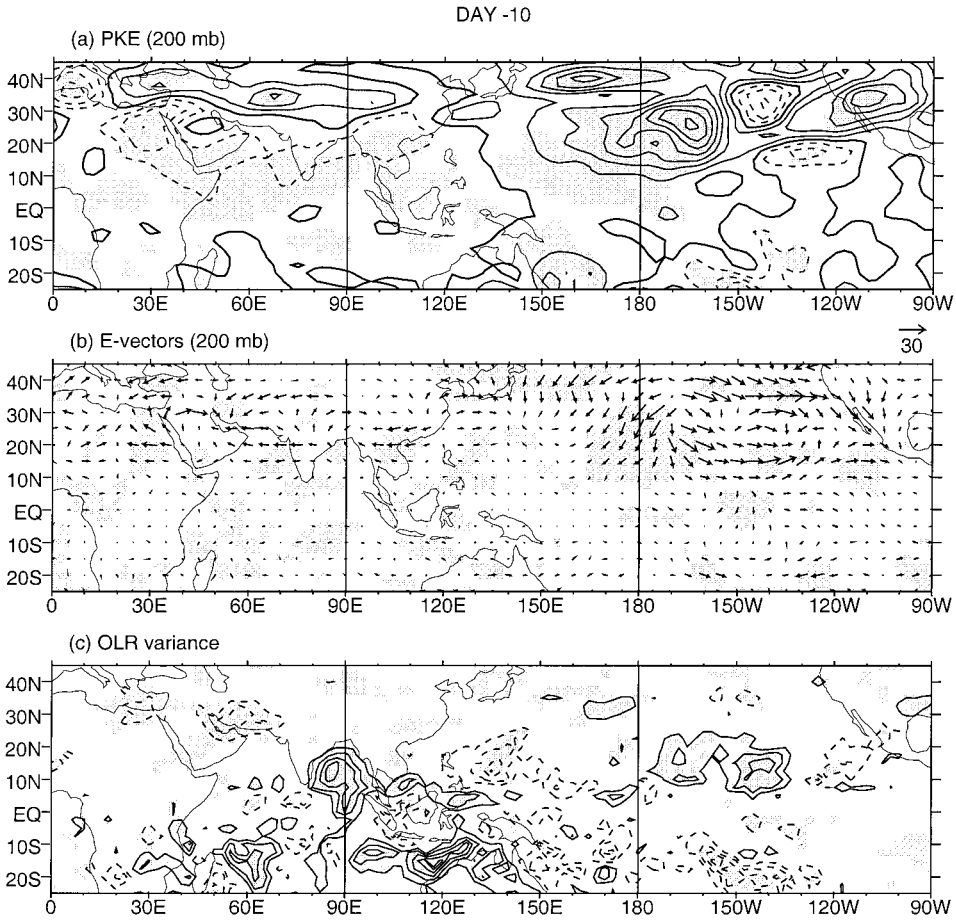

FIG. 5. Lagged regression maps of high-frequency (6–25 day) transients at day −10 for a (30–70-day filtered) OLR anomaly of −20 W m^{-2} over the region (15°S–5°N, 140°–160°E). (a) The 200-mb PKE. Contour interval is 4 $m^2 s^{-2}$. Positive (negative) contours are solid (dashed), and the zero contour is thickened. Shading indicates local significance at the 95% level. (b) The 200-mb E vectors. Reference vector is 30 $m^2 s^{-2}$. Shading indicates local significance of either component at the 95% level. (c) OLR variance. Contour interval is 50 $W^2 m^{-4}$. Positive (negative) contours are solid (dashed), and the zero contour is suppressed. Shading indicates local significance at the 95% level.

to 16% of the variance of the high-frequency convective variability on intraseasonal timescales is linearly related to the MJO.

Although there is enhanced high-frequency convective variability over the warm pool region, there are *negative* PKE anomalies over the region (Fig. 5a). Although small, these anomalies are statistically significant, even over the Bay of Bengal where the positive anomalies in the high-frequency convective variability are strongest. The E vector anomalies are very small over the warm pool region and show no consistent pattern (Fig. 5b). This is to be expected, as easterlies almost always cover the whole region (Fig. 2a) and mean E-vector amplitudes are very small (Fig. 3).

The situation has reversed a half cycle later, on day +10 (Fig. 6). Over the warm pool, reduced convection on the 30–70-day timescale (Fig. 4c) is coincident with reduced off-equatorial high-frequency convective variability (Fig. 6c) but weakly enhanced PKE (Fig. 6a), especially over the Bay of Bengal and southeast Asia. Once again, E-vector anomalies over the warm pool region are very small (Fig. 6b).

As discussed in section 1, tropical–extratropical interaction has been proposed as a possible mechanism for the initiation of the convective cycle of an MJO in the Indian Ocean. If it can be shown that there is an enhancement of high-frequency transients propagating into the Indian Ocean region at the beginning of a typical MJO, this would lend further evidence to the existence of an extratropical forcing mechanism for the MJO.

The slowly evolving basic state of the MJO on day +20 is such that convection on the 30–70-day timescale is just developing in the Indian Ocean; that is, the next cycle of the MJO is beginning (Fig. 4d). Figure 7 shows the behavior of the high-frequency transients on day +20. The enhanced convection on the equator, centered at 75°E (Fig. 4d), is also a region of enhanced high-frequency convective variability (Fig. 7c). In contrast

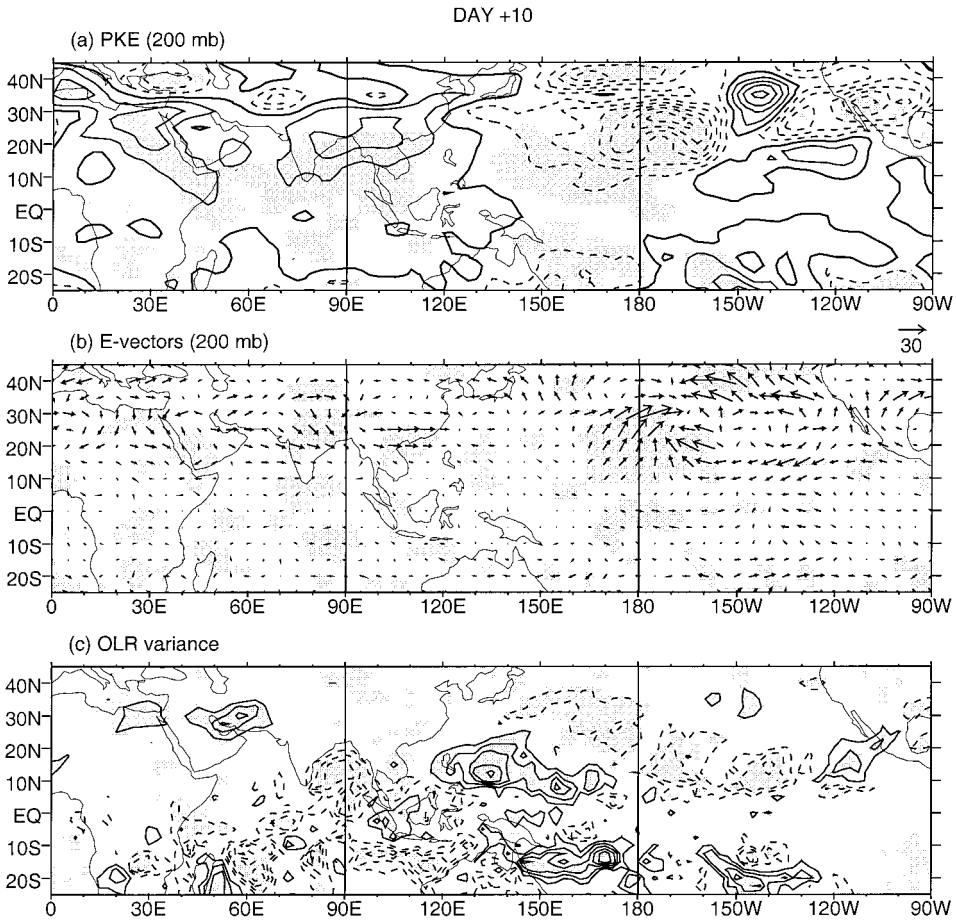

FIG. 6. As in Fig. 5 but for day +10.

to the behavior over the warm pool described above, a consistent signal between the PKE and E-vector fields is present. A belt of statistically significant PKE anomalies covers the northern Indian Ocean, India, and part of southeast Asia (Fig. 7a). This enhanced PKE is coincident with an enhancement of eddy activity propagating into the Indian Ocean, as shown by the anomalous southward- and eastward-pointing E vectors in Fig. 7b. These anomalous E vectors are in approximately the same direction as the mean E vectors over the region (Fig. 3) and, therefore, indicate an anomalous pulse or packet of high-frequency waves over the region during this phase (day +20) of the MJO. Hence, it appears that extratropical forcing might play a role in the initiation of the MJO. However, the relative importance of this role with respect to other potential initiation mechanisms is still unclear.

b. Central and eastern Pacific sector

On day −10 the MJO is in a state of enhanced convection over the east Indian Ocean and the maritime continent. Near the date line, the Asian–Pacific jet is retracted and there are westerly anomalies in the Tropics (Fig. 4a). The high-frequency transients at this phase of the MJO show statistically significant, positive 200-mb PKE anomalies over the central Pacific, indicating an increase in wave activity over the region (Fig. 5a). There is a relative minimum in the positive PKE anomalies along 35°N, indicating that the variability in the wave activity is located on the flanks of the jet rather than in the jet itself [note that the mean PKE (Fig. 2c) does have a maximum at the latitude of the jet core (35°N), though the area of largest mean PKE is downstream from the jet exit region, over the eastern Pacific]. Local correlations in the region are up to 0.46 (not shown); hence, up to 21% of the variance of the high-frequency PKE on intraseasonal timescales is accounted for by this linear relationship with the MJO.

Figure 5b shows statistically significant, southward-pointing E-vector anomalies over the central Pacific at this phase of the MJO. These anomalies are in approximately the same direction as the mean E vectors (Fig. 3) and indicate an enhancement in equatorward-propagating eddy activity near the date line. There are also large E-vector anomalies eastward along and to the north of the ITCZ into the eastern Pacific. Consistent with this anomalously strong equatorward-propagating eddy

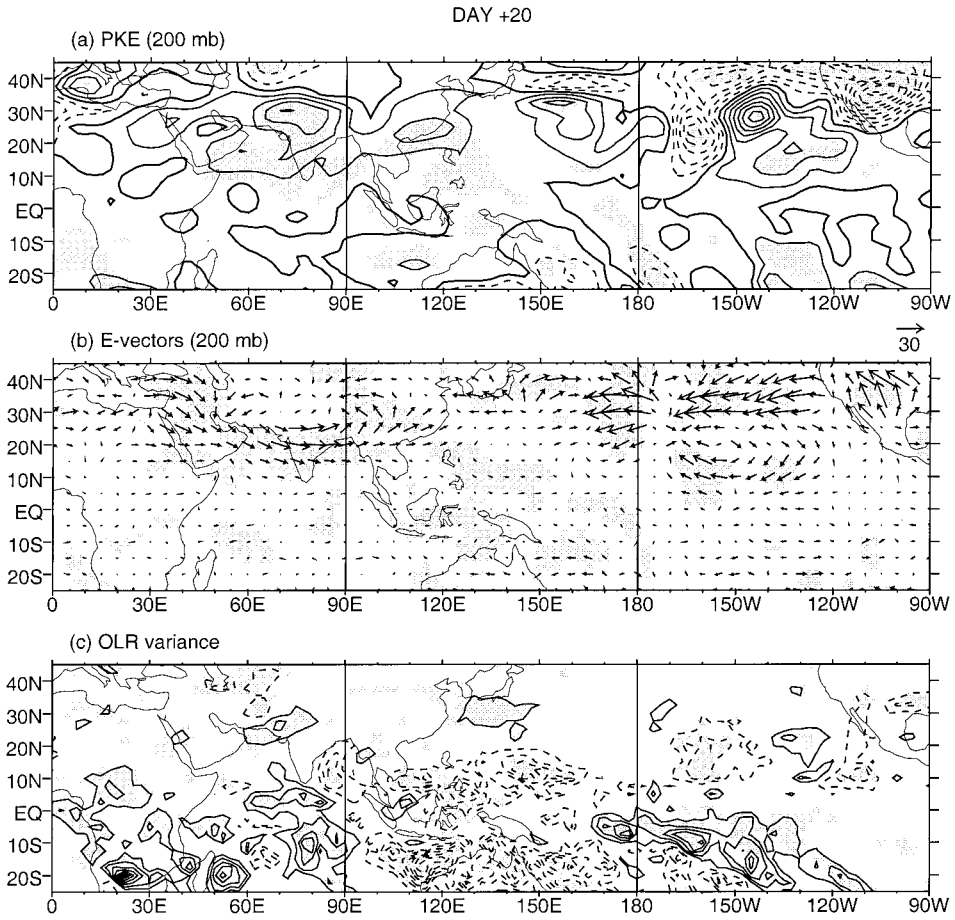

FIG. 7. As in Fig. 5 but for day +20.

activity, there is enhanced high-frequency convective variability in the ITCZ region of the central Pacific from 170° to 130°W (Fig. 5c).

This enhanced high-frequency convective variability over the central Pacific ITCZ on day −10 of the MJO does not, by itself, imply that there will be a convective signal on the slowly varying 30–70-day timescale in this region. However, inspection of the day −10 regression map of 30–70-day filtered OLR (Fig. 4a) indeed reveals a region of enhanced convection along and to the north of the ITCZ at 160°W, which is coincident with the signal of enhanced high-frequency convective variability described above. It seems likely that the two are related, and the enhanced high-frequency convective variability in Fig. 5c projects onto intraseasonal timescales and leads to the enhanced slowly varying convective anomaly in Fig. 4a. This may have important consequences for the evolution of the MJO, as the slowly varying convective anomaly or diabatic heating anomaly may subsequently force, or initiate, a dynamical response on the same timescale.

TABLE 2. As in Table 1 but for the high-frequency transients; 200-mb PKE, *x* and *y* components of the E vector (E_x and E_y), and OLR variance calculated from 6–25-day filtered data, then passed through a 30–70-day filter and regressed against the 30–70-day filtered reference OLR time series. If the field is globally significant at the 90%, 95%, or 99% level, this is indicated by a bracketed superscript in the relevant cell.

Day	PKE (200 mb)	E_x (200 mb)	E_y (200 mb)	OLR variance
−10	$17.2^{(99)}$	$8.9^{(90)}$	$10.0^{(95)}$	$12.6^{(99)}$
0	$9.1^{(90)}$	7.7	6.8	$13.7^{(99)}$
+10	$17.4^{(99)}$	$10.4^{(95)}$	$10.5^{(95)}$	$14.3^{(99)}$
+20	$12.3^{(99)}$	$10.9^{(95)}$	$9.3^{(95)}$	$13.6^{(99)}$

The regression maps of the high-frequency transients, approximately half a cycle later, on day +10, are shown in Fig. 6. The situation is approximately opposite to that at day −10 (Fig. 5). The central Pacific is now a region of reduced PKE, with the largest (negative) anomalies once again flanking the jet (Fig. 6a). The anomalous E vectors near the date line point northward in the opposite direction to the mean E vectors, indicating a reduction in equatorward-propagating wave activity (Fig. 6b). Consistently, the high-frequency convective variability is also reduced in the ITCZ region of the central Pacific (Fig. 6c). This reduction in high-frequency convective variability appears to project back onto intraseasonal

timescales, as the positive 30–70-day OLR anomaly centered at 15°N, 165°W in Fig. 4c.

The original hypothesis of this paper appears, therefore, to have been borne out. Slowly varying changes to the climatological mean basic state through an MJO life cycle are accompanied by a modulation of the amplitude and propagation characteristics of the high-frequency transient eddies, and the intensity of the high-frequency convective variability, over the ITCZ of the central Pacific. This modulation is highly statistically significant and accounts for up to 21% of the variance (locally) of the relevant variables.

The MJO has been shown to be associated with a modulation of the high-frequency transients in the Pacific, but is it the dominant control on intraseasonal modulation? To answer this question, a further regression analysis was performed. A reference time series of high-frequency convective variability over the eastern Pacific ITCZ was constructed by area averaging the variance of 6–25-day filtered OLR over a 20° × 20° box (5°–25°N, 150°−130°W). This time series was then passed through the 30–70-day filter, to isolate the intraseasonal modulation of the high-frequency convective variability. Gridpoint fields of 30–70-day filtered OLR and 200-mb zonal wind were then regressed against this reference time series. The regression maps (not shown) were very similar to the MJO life cycle of Fig. 4, indicating that the principal mode of intraseasonal variability of the high-frequency transients in the eastern Pacific is, indeed, the MJO.

Previous work (Kiladis and Weickmann 1992b) has found that the high-frequency waves have a period around 12 days, hence the choice of the 6–25-day filter used here. However, it is possible that waves with periods less than the 6-day cutoff may also be important in the evolution of the MJO. Therefore, the same diagnostics were calculated using 25-day high-pass filtered data instead of the 6–25-day bandpassed data. In general, the anomaly patterns calculated from the 25-day high-passed data have qualitatively the same shape as those calculated from the 6–25-day bandpassed data. However, the PKE anomalies over the Pacific have approximately doubled in magnitude, implying that there is substantial eddy activity that is coherently related to the MJO, arising from waves with periods less than 6 days (the cross terms between the 6-day high-pass and the 6–25-day bandpass data were small). On the other hand, the E-vector anomalies calculated from the 25-day high-passed data were very similar in both direction and magnitude to those calculated from the 6–25-day bandpassed data. This implies that, although the amplitude of the higher frequency (<6 day) waves is modulated by the MJO in a similar way to the 6–25-day waves, the propagation characteristics of these higher frequency waves do not appear to be coherently related to the MJO.

The 25-day high-passed OLR variance anomalies are approximately double the magnitude of the 6–25-day OLR variance anomalies over the warm pool. This is consistent with the enhanced synoptic variability over the warm pool during the wet phase of the MJO, as reported by Hendon and Liebmann (1994), Chen et al. (1996), Sui et al. (1997), and others. However, over the central and eastern Pacific ITCZ regions, the 25-day high-passed OLR variance anomalies are very similar to those calculated from the 6–25-day bandpassed data, implying that the MJO modulates or interacts with convection primarily on the 6–25-day timescale in this region but not with convection on shorter timescales (except for perhaps the diurnal cycle, which was excluded from this analysis by the use of daily averaged data).

6. Rossby wave dynamics

The regression analysis of the previous section has revealed a coherent relationship between the slowly evolving basic state of the MJO and high-frequency wave activity and convective variability, especially over the central Pacific ITCZ region. In this section, this relationship is interpreted using barotropic Rossby wave theory (e.g., Hoskins and Ambrizzi 1993). For a given phase of the MJO, the basic state through which the high-frequency waves propagate is constructed by the compositing procedure described in section 2d.

Consistent with the regression analysis (Fig. 4a), the composite-mean 200-mb total zonal wind field for the day −10 phase (Fig. 8a) shows a westward shift of the Asian–Pacific jet (stronger over Asia, weaker over the Pacific), a westward-retracted area of tropical easterlies over the warm pool (the zero wind line is west of the date line), and weaker equatorial westerlies over the eastern Pacific, as compared to that for the day +10 phase (Fig. 8b). These features can be seen more clearly in the difference field (Fig. 8c), which is very similar to the difference between the regressed fields of 30–70-day filtered 200-mb zonal wind (Figs. 4a–c).

The total stationary wavenumber fields, for the day −10 and day +10 phases of the MJO, are calculated from the appropriate 200-mb total zonal wind fields described above and are shown in Figs. 9a and 9b, respectively. In the day −10 phase, the retracted Asian–Pacific jet over the Pacific leads to a much weaker, leakier waveguide. The total wavenumber in the Asian–Pacific jet exit region has decreased to about 5. The high-frequency waves that propagate into the central and eastern Pacific ITCZ region have typical wavenumbers of 5–6 (Kiladis and Weickmann 1992b); hence, these waves will not be so tightly confined to the jet exit region in this phase of the MJO. This could account for the relative minimum in the high-frequency PKE anomalies in the jet core region itself (Fig. 5a) and the large, positive high-frequency PKE anomalies on either side of the jet.

The region of imaginary stationary wavenumber, corresponding to the region of mean easterlies over the warm pool, has retracted westward, allowing waves to propa-

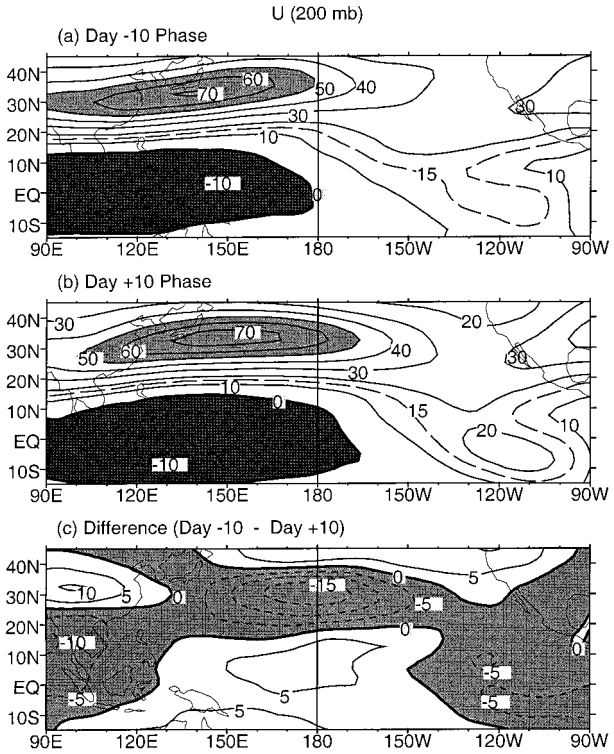

FIG. 8. Composite-mean 200-mb total zonal wind for the (a) day −10 phase of the MJO life cycle (averaged from day −15 to day −5 of each individual MJO event), (b) day +10 phase (averaged from day +5 to day +15). Contour interval is 10 m s^{-1}, and the extra 15 m s^{-1} contour is shown by a long-dashed line. Values above 50 m s^{-1} (below 0 m s^{-1}) are shaded lightly (darkly). (c) Difference field (a)–(b). Contour interval is 5 m s^{-1} and negative values are shaded. In all diagrams, positive (negative) contours are solid (dashed), and the zero contour is thickened.

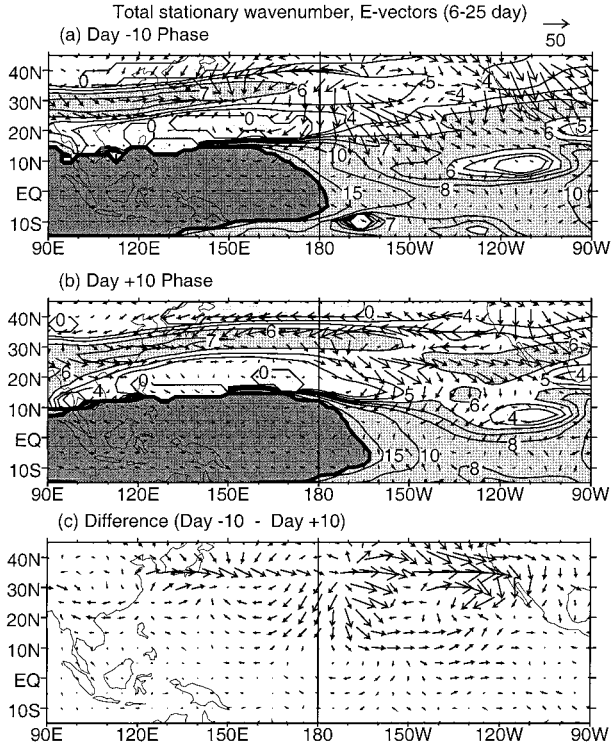

FIG. 9. Composite-mean 200-mb total stationary wavenumber fields and high-frequency (6–25 day) E-vector fields for the (a) day −10 and (b) day +10 phases of the MJO. (c) E-vector difference field (a)–(b). Conventions as in Fig. 3.

gate into the deep Tropics near the date line. The mean 200-mb total E-vector field of the 6–25-day filtered data for the day −10 phase is also shown in Fig. 9a. Consistent with the weaker waveguide in the Pacific jet exit and the retracted region of imaginary total wavenumber, there are large southward-pointing E vectors near the date line, indicating equatorward-propagating waves.

Figure 9b shows the total stationary wavenumber and mean E vectors for the day +10 phase of the MJO. The Pacific jet is extended and there is an almost continuous waveguide, with total wavenumber greater than 6 across the Pacific. The ''forbidden'' region of imaginary total wavenumber, or mean easterlies, over the warm pool, has expanded eastward to 165°W. Consistent with this change in basic state, the behavior of the high-frequency transients has been altered such that southward-pointing E vectors near the date line have been almost eliminated.

Over the northeast Pacific and North America (20°–40°N, 130°–90°W) during the day −10 phase, total stationary wavenumber increases to the south (Fig. 9a). Consistent with this distribution of total wavenumber, E vectors also point approximately southward over the northeast Pacific. During the day +10 phase the waveguide is almost continuous across the whole Pacific, and correspondingly the E vectors are aligned approximately east–west, along the axis of the waveguide. Along the northern flank of the waveguide, the E vectors point westward, indicating zonally elongated eddies, whereas along the southern flank they point eastward, indicating meridionally elongated eddies. Figure 9c shows the difference in the E-vector fields between the day −10 and day +10 phases. It emphasizes the features described above and is similar to the difference in the regressed E-vector fields of day −10 and day +10 (i.e., Figs. 5b–6b).

The westerly anomalies of 10 m s^{-1} at the jet entrance region (35°N, 90°–110°E), together with easterly anomalies to the north and south (Fig. 8c), strengthen the meridional vorticity gradient and lead to a slightly stronger waveguide over Asia, in the day −10 phase, compared to the day +10 phase (Figs. 9a,b). However, there appears to be little corresponding change in the behavior of the high-frequency waves, as the E-vector anomalies in this region are small (Fig. 9c). Over the equatorial eastern Pacific, even though the near-equatorial westerly maximum is weakened with easterly anomalies around −5 m s^{-1} (Fig. 9c), there is little change in the stationary wavenumber pattern (Figs. 9a,b) and in the E-vector field (Fig. 9c).

The southward-pointing E vectors over the central Pacific near the date line in the day −10 phase (Fig.

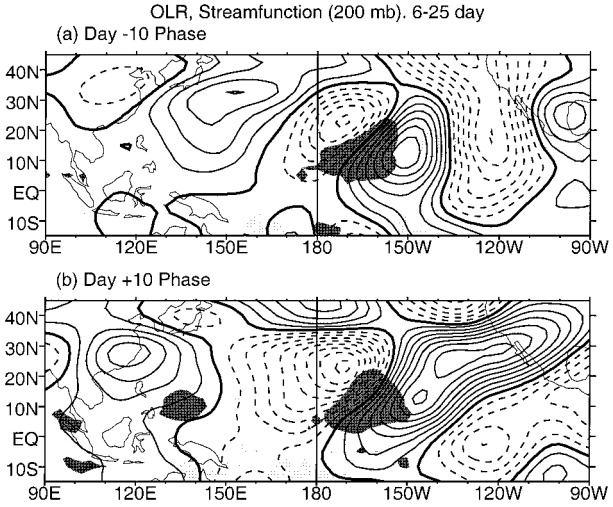

FIG. 10. Simultaneous regression maps of high-frequency (6–25 day) filtered OLR and 200-mb streamfunction for an OLR anomaly of -25 W m^{-2} averaged over (5°–15°N, 170°–160°W) for (a) day -10, (b) day $+10$ phases of the MJO. OLR is shaded darkly below -10 W m^{-2} and lightly above $+10$ W m^{-2}. Streamfunction contour interval is 10^6 m^2 s^{-1}. Positive (negative) contours are solid (dashed), and the zero contour is thickened.

9a), and the zonally oriented E vectors between 25° and 40°N over the eastern Pacific in the day $+10$ phase (Fig. 9b) indicate the different propagation characteristics of the high-frequency waves in the two opposite phases of the MJO. To further highlight these different characteristics, 6–25-day filtered 200-mb streamfunction and OLR are regressed against 6–25-day filtered OLR in a $10° \times 10°$ box over the central Pacific ITCZ (5°–15°N, 170°–160°W). This box covers a region of enhanced high-frequency convective variability on day -10 of the MJO (Fig. 5c) and reduced high-frequency convective variability during the opposite, day $+10$, phase of the MJO (Fig. 6c). It is also in the region of strong forcing of ITCZ convection studied by Kiladis and Weickmann (1992b, 1997). Separate regressions are performed over the day -10 and day $+10$ MJO phases (i.e., two nonoverlapping periods of 253 days each), and the lag 0 regression maps are shown in Figs. 10a and 10b, respectively.

Both figures show a northwest–southeast-oriented wave train and enhanced convection (negative OLR anomalies) in the ascent region ahead of the trough. Lagged regression maps (not shown) show the familiar eastward and equatorward phase and group propagation of the waves in both cases. However, there are also marked differences. The waves in the day -10 phase (Fig. 10a) begin to propagate equatorward well to the west of the date line, as shown by the southwest–northeast-oriented phase lines east from 160°E. This is consistent with the southward component to the E vectors in this region in this phase (Fig. 9a). West of the date line in the day $+10$ phase, the waves are weaker and have little horizontal tilt (Fig. 10b). In a consistent manner, the E vectors in this region are weaker than in the day -10 phase and have a very small meridional component (Fig. 9b). In the subtropics along 35°N, the waves in the day $+10$ phase (Fig. 10b) are more zonally oriented than those in the day -10 phase (Fig. 10a), and the zonal scale is larger than the meridional scale. This accounts for the strong westward-pointing E vectors in this region in the day $+10$ phase and is consistent with propagation along the almost continuous waveguide across the Pacific in this phase (Fig. 9b).

7. Case studies

The regression and composite analyses of the previous two sections have established the ''average'' behavior of the high-frequency transients in different phases of the MJO. Additionally, the 23 MJO events used in the composite were examined to determine whether the relationships can be detected in individual cases.

The 30–70-day filtered fields were subjectively inspected for the following key anomalies on each of the 23 day -10 occurrences: OLR for a dipole anomaly with enhanced convection over the maritime continent and suppressed convection over the SPCZ, 200-mb zonal wind for a retracted Asian–Pacific jet (easterly anomalies) and equatorial westerly anomalies in the central Pacific, high-frequency PKE for enhanced wave activity over the Northern Hemisphere central Pacific (near the date line), high-frequency E vectors for southward-pointing anomalies over the central Pacific, and high-frequency OLR variance for enhanced variability over the central Pacific ITCZ. The same fields on the 23 day $+10$ occurrences were inspected for anomalies of the opposite sign.

Even though there was considerable variability between the different cases, the key anomalies were observed in the majority of cases. When the cases were restricted to those with the ''correct'' basic-state anomalies—that is a retracted Asian–Pacific jet and equatorial westerly anomalies near the date line on day -10 and the opposite on day $+10$—the anomalies in PKE, E vectors, and high-frequency convective variability agreed even more clearly with those from the regression analyses.

The quadratic quantities of the high-frequency transients described above (i.e., PKE, E vectors, and OLR variance) give information only about their modulation by the MJO. All phase information of the high-frequency fields has been lost. To show an example of a typical evolution of transients during different phases of an MJO, the daily fields of 6–25-day filtered OLR and 200-mb streamfunction during one particular event, in January–February 1982, are examined in Fig. 11. Day 0 (i.e., the minimum in the warm pool OLR reference time series) for this event is 26 January 1982. The 30–70-day filtered fields of OLR and 200-mb zonal wind, and of high-frequency PKE, E vectors, and OLR variance, on 16 January 1982 (day -10) and on 5 February

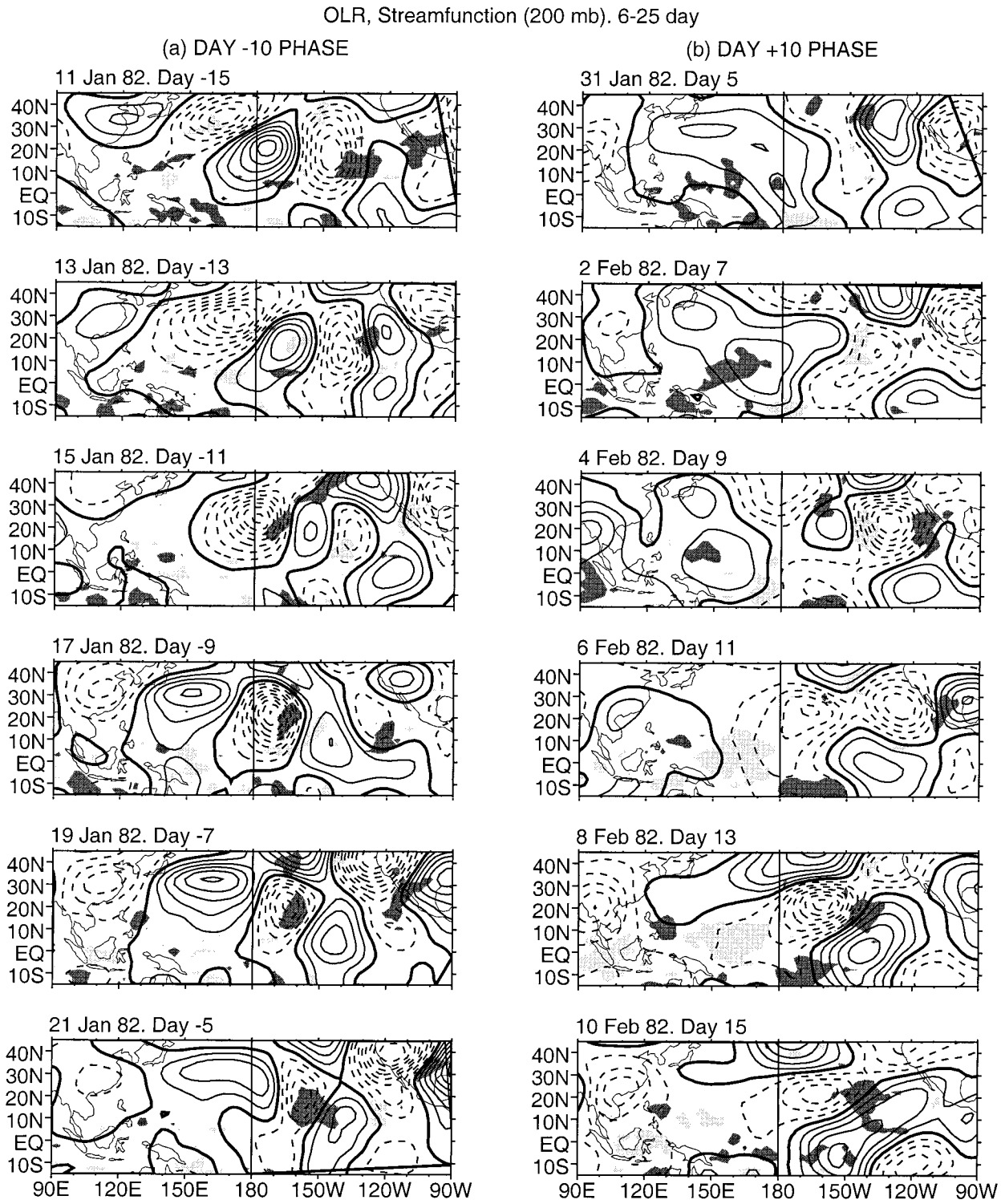

FIG. 11. High-frequency (6–25 day) filtered OLR and 200-mb streamfunction fields, every 2 days, during the MJO of Jan–Feb 1982. (a) Day −10 phase, from 11 to 21 Jan 1982 (day −15 to day −5). (b) Day +10 phase, from 31 Jan to 10 Feb 1982 (day +5 to day +15). OLR is shaded darkly below −30 W m^{-2} and lightly above 30 W m^{-2}. Streamfunction contour interval is 5×10^6 m^2 s^{-1}. Positive (negative) contours are solid (dashed) and the zero contour is thickened.

1982 (day +10), are very similar to the respective regression fields described in section 5b.

Figure 11a shows the 6–25-day filtered OLR and 200-mb streamfunction fields every two days, for 11–21 January 1982 (day −15 to day −5)—that is, the day −10 phase of this event. Consistent with the positive 30–70-day filtered PKE anomalies and southward-pointing E-vector anomalies for 16 January 1982, there is strong equatorward propagation of wave activity around the date line throughout this period, as shown by the southwest–northeast tilt to the waves. There is enhanced convection (negative OLR anomalies) ahead of the troughs, as described by Kiladis and Weickmann (1992b).

Twenty days later, the situation is rather different. Figure 11b shows the 6–25-day filtered OLR and 200-mb streamfunction, every two days, from 31 January 1982 to 10 February 1982 (day +5 to day +15; the day +10 phase). During this phase of the MJO there is reduced high-frequency PKE and convective variability over the Pacific near the date line. This is evident from the lack of any strong wave activity near the date line for most of this period.

Farther east, near 150°W, equatorward-propagating wave activity is similar in both the day −10 and the day +10 phases of this particular MJO. This is representative of the mean MJO, as indicated by the lack of meridional E-vector anomalies in the immediate vicinity of 20°N, 150°W (Figs. 5b, 6b, 9c).

8. Discussion

The interaction between high-frequency (6–25 day) transients and the MJO has been investigated using satellite OLR data and 200-mb fields from the NCEP–NCAR reanalyses and interpreted in the framework of barotropic Rossby wave theory. According to this theory, the Asian–Pacific jet acts as a waveguide, and the tropical easterlies are a forbidden region for Rossby waves. Under mean DJF conditions, both the Asian–Pacific jet waveguide and the forbidden region of tropical easterlies extend east of the date line, to around 160°W, and equatorward propagation of high-frequency transients near the date line is weak.

In the phase of the MJO denoted as day −10 in this study, with enhanced convection over the east Indian Ocean and Indonesia, and reduced convection over the SPCZ, the Asian–Pacific jet exit is weak, and the transition region between upper-tropospheric tropical easterlies over the warm pool and equatorial westerlies over the eastern Pacific is located to the west of the date line. Under these conditions, Rossby waves (high-frequency transients) can leak out of the weaker waveguide and propagate into the deep Tropics near the date line.

PKE and E-vector diagnostics of the high-frequency transients at 200 mb during this phase of the MJO show that this is indeed the case. There are positive high-frequency PKE anomalies over most of the central Pacific, except in the jet core itself, indicative of the wave activity propagating out of the jet. Anomalous E vectors point southward near the date line in the Northern Hemisphere, indicative of the anomalous equatorward propagation of the transients in this region.

Previous work by Kiladis and Weickmann (1992b, 1997), among others, has shown that deep convection in the tropical central and eastern Pacific, on the 6–30-day timescale, is induced by equatorward-propagating waves. The convection arises in the regions of ascent and reduced static stability ahead of the troughs in the wave trains. Hence the anomalous, equatorward-propagating high-frequency waves near the date line in the day −10 phase of the MJO may be expected to induce anomalous convection on the 6–25-day timescale. The positive anomalies in high-frequency OLR variance over the tropical central Pacific in this phase of the MJO are consistent with this hypothesis.

During the opposite or day +10 phase of the MJO, a reversed situation is found. Convection is reduced over the east Indian Ocean and Indonesia, and enhanced over the SPCZ, on the 30–70-day timescale. The Asian-Pacific jet is now extended, and an almost continuous waveguide extends across the Pacific. The forbidden region of tropical upper-tropospheric easterlies above the warm pool is now also extended east of the date line. Consistent with these changes in basic state, E vectors for this phase of the MJO show little equatorward propagation near the date line and more zonal propagation along the stronger, more extensive waveguide over the North Pacific. The reduced wave activity in the central Pacific ITCZ does not induce as much transient convection, as reflected by a negative anomaly in high-frequency OLR variance.

The anomalies in high-frequency convective variability or OLR variance over the central Pacific ITCZ, positive (negative) in the day −10 (+10) phase, appear to project back onto intraseasonal timescales and form an integral part of the slowly varying diabatic heating field of the MJO. Hence, there appears to be a two-way interaction between the high-frequency transients and the more slowly varying MJO over the central Pacific. When the MJO convection is in the east Indian Ocean, the basic state allows the high-frequency transients to propagate into the deep Tropics near the date line. These transients then induce enhanced high-frequency convective variability, which is seen on the MJO timescale as a slowly varying positive diabatic heating anomaly. This heating anomaly may then force, or initiate, a low-frequency dynamical response as part of the MJO. Modeling studies should help to determine the nature of this two-way interaction. Note that such causal relationships can only be inferred, not proven, from our approach here. However, as they are supported by predictions from Rossby wave theory, this type of approach appears to be justified.

This scenario for the development of MJO convection along the ITCZ in the Northern Hemisphere can be compared to the development of MJO convective anomalies

along the SPCZ in the Southern Hemisphere (Matthews et al. 1996). In their study, large-scale deep convection over Indonesia, associated with the MJO, generated a subtropical Rossby wave train in the Southern Hemisphere. The deep ascent ahead of, and induced by, an upper-level trough in this wave train then forces, or triggers, deep convection over the SPCZ. Hence the MJO convection over the SPCZ arises as a direct dynamical response to the MJO convection over Indonesia.

The situation in the Northern Hemisphere, examined in the present study, is somewhat different. Although the changes to the basic state (i.e., the retraction of the Pacific jet and the region of equatorial upper-tropospheric easterlies over the warm pool in the day −10 phase) can be explained as a direct response to forcing by the MJO convection over the Indian Ocean and Indonesia (Ting and Sardeshmukh 1993; Jin and Hoskins 1995), the subsequent development of MJO convection over the ITCZ does not appear to be directly linked to a large-scale Rossby wave response. Instead the anomalous basic state allows high-frequency waves to propagate equatorward near the date line. These high-frequency transients induce enhanced convection on a similar timescale, which projects back onto the longer, intraseasonal timescale and produces an MJO convective anomaly over the ITCZ. Hence, the interaction between the two timescales of the MJO and the high-frequency transients appears to be important over the ITCZ in the central Pacific.

The ray-tracing theory and the use of the total stationary wavenumber as a useful diagnostic rely on a separation of scales between the variations in the time-mean basic state and transient waves. Hoskins and Ambrizzi (1993) conceded that the condition of spatial-scale separation is violated, and in this study there is not a strict separation of temporal scales. The different basic states during an MJO life cycle remain approximately constant for about a quarter-cycle, or 12 days, which is the same as the average period of the transient waves. Hence, during a particular phase of the MJO, there is only time for one transient wave to propagate through a region and feel the influence of the change to the basic state. It is a testament to the robustness and general applicability of the theory that consistent results are obtained.

In addition to changes in the basic state and subsequent changes to the propagation characteristics of the high-frequency transients, the source of the transients also needs to be considered. The high-frequency waves appear to have their origins in the Asian jet. On the 6–30-day timescale, convection over the east Indian Ocean in Northern Hemisphere winter is associated with a wave train in the Asian jet. The convective anomaly peaks before the circulation anomalies, indicating that the wave train is forced by the tropical convection (Kiladis and Weickmann 1992a, 1997). The wave train propagates along the jet and then equatorward over the eastern Pacific and forces deep convection in the ITCZ about two days later (Meehl et al. 1996). The modeling study of Slingo (1998) also supports this sequence of events.

This interaction between convection over the Indian Ocean and convection over the eastern Pacific ITCZ may be relevant to the MJO. In the day −10 phase, there is enhanced convection on the 6–25-day timescale (positive OLR variance anomalies) over the east Indian Ocean (Fig. 5c). According to the scenario described above, this will induce enhanced high-frequency wave activity, as indicated by the positive high-frequency PKE anomalies in the Asian jet (Fig. 5a). The enhanced convective variability over the east Indian Ocean may not be the only explanation for the enhanced wave activity in the Asian jet. On the 30–70-day timescale, the Asian jet is stronger at day −10 (westerly anomalies near 35°N cover the whole of Asia in Fig. 4a). Hence the Asian jet waveguide is stronger at this phase of the MJO (Fig. 9a) and transients of wavenumbers 6–7 will be more tightly constrained to propagate along the Asian jet. Additionally, the stronger Asian jet will be more baroclinically unstable and the enhanced PKE observed in the jet may arise from the stronger baroclinic instability of the basic state. However, the positive high-frequency PKE anomalies during the day −10 phase of the MJO, although they cover the whole Asian jet region, are only statistically significant over a small region. Hence, the changes in the wave source during the MJO is likely to be of secondary importance compared to the changes in the basic state and the propagation characteristics of the high-frequency waves over the Pacific.

There is also evidence for interaction between high-frequency transients and the MJO during the initiation phase of the MJO in the Indian Ocean. Anomalous high-frequency wave activity propagates from the Middle East into the Indian Ocean region (Fig. 7b), just as the slowly varying convection of the MJO is developing there (Fig. 4c). Propagation of extratropical waves into the tropical Indian Ocean region has been shown to initiate the MJO in case studies (Hsu et al. 1990) and simple modeling studies (Bladé and Hartmann 1993). The regression analysis of this study has established that such tropical–extratropical interaction is representative of the typical MJO in northern winter. However, a causal link between the high-frequency waves and convection over the Indian Ocean has not been established. It is not clear either why there should be this anomalous high-frequency wave activity over the Indian Ocean during this phase of the MJO. The tropical zonal wind anomalies are westerly, but weak, and therefore changes to the basic state will be small. Alternatively, the extratropical source of the high-frequency transients may have changed rather than the propagation characteristics of the transients themselves. One possible candidate is the enhanced convection over equatorial South America during this phase and an associated increase in high-frequency convective variability (not shown). This may act as an enhanced source of wave activity that quickly disperses downstream over the Indian Ocean region.

Acknowledgments. The authors thank Brian Hoskins, Klaus Weickmann, Matthew Wheeler, and Tercio Ambrizzi for helpful discussions and comments. The OLR and NCEP–NCAR reanalysis data were provided through the NOAA Climate Diagnostics Center (http://www.cdc.noaa.gov). This research was supported by the Pan-American Climate Studies Program, under project GC95-820, sponsored by NOAA's Office of Global Programs.

REFERENCES

Ambrizzi, T., 1994: Rossby wave propagation on EL Niño and La Niña basic flows. *Rev. Bras. Meteor.,* **9,** 54–65.

Arkin, P. A., and P. J. Webster, 1985: Annual and interannual variability of tropical–extratropical interaction: An empirical study. *Mon. Wea. Rev.,* **113,** 1510–1523.

——, and P. E. Ardanuy, 1989: Estimating climatic-scale precipitation from space: A review. *J. Climate,* **2,** 1229–1238.

Bladé, I., and D. L. Hartmann, 1993: Tropical intraseasonal oscillations in a simple nonlinear model. *J. Atmos. Sci.,* **50,** 2922–2939.

Chang, E. K. M., 1993: Downstream development of baroclinic waves as inferred from regression analysis. *J. Atmos. Sci.,* **50,** 2038–2053.

Chen, S. S., and R. A. Houze, 1997: Diurnal variation and life-cycle of deep convective systems over the tropical Pacific warm pool. *Quart. J. Roy. Meteor. Soc.,* **123,** 357–388.

——, ——, and B. E. Mapes, 1996: Multiscale variability of deep convection in relation to large-scale circulation in TOGA COARE. *J. Atmos. Sci.,* **53,** 1380–1409.

Duchon, C. E., 1979: Lanczos filtering in one and two dimensions. *J. Appl. Meteor.,* **18,** 1016–1022.

Hendon, H. H., and B. Liebmann, 1994: Organization of convection within the Madden–Julian Oscillation. *J. Geophys. Res.,* **99,** 8073–8083.

——, and M. L. Salby, 1994: The life cycle of the Madden–Julian Oscillation. *J. Atmos. Sci.,* **51,** 2225–2237.

Hoskins, B. J., and T. Ambrizzi, 1993: Rossby wave propagation on a realistic longitudinally varying flow. *J. Atmos. Sci.,* **50,** 1661–1671.

——, I. N. James, and G. H. White, 1983: The shape, propagation and mean-flow interaction of large-scale weather systems. *J. Atmos. Sci.,* **40,** 1595–1612.

Hsu, H. H., B. J. Hoskins, and F. F. Jin, 1990: The 1985/86 intraseasonal oscillation and the role of the extratropics. *J. Atmos. Sci.,* **47,** 823–839.

Janowiak, J. E., P. A. Arkin, P. Xie, M. L. Morrissey, and D. R. Legates, 1995: An examination of the East Pacific ITCZ rainfall distribution. *J. Climate,* **8,** 2810–2823.

Jin, F.-F., and B. J. Hoskins, 1995: The direct response to tropical heating in a baroclinic atmosphere. *J. Atmos. Sci.,* **52,** 307–319.

Kalnay, E., and Coauthors, 1996: The NCEP/NCAR 40-Year Reanalysis Project. *Bull. Amer. Meteor. Soc.,* **77,** 437–471.

Kiladis, G. N., 1998: An observational study of Rossby waves linked to convection over the eastern tropical Pacific. *J. Atmos. Sci.,* **55,** 321–339.

——, and K. M. Weickmann, 1992a: Circulation anomalies associated with tropical convection during northern winter. *Mon. Wea. Rev.,* **120,** 1900–1923.

——, and ——, 1992b: Extratropical forcing of tropical Pacific convection during northern winter. *Mon. Wea. Rev.,* **120,** 1924–1938.

——, and S. B. Feldstein, 1994: Rossby wave propagation into the Tropics in two GFDL general circulation models. *Climate Dyn.,* **9,** 245–252.

——, and K. M. Weickmann, 1997: Horizontal structure and seasonality of large-scale circulations associated with submonthly tropical convection. *Mon. Wea. Rev.,* **125,** 1997–2013.

Killworth, P. D., and M. E. McIntyre, 1985: Do Rossby wave critical layers absorb, reflect, or over-reflect? *J. Fluid Mech.,* **161,** 449–492.

Knutson, T. R., and K. M. Weickmann, 1987: 30–60 day atmospheric oscillations: Composite life cycles of convection and circulation anomalies. *Mon. Wea. Rev.,* **115,** 1407–1436.

Lau, K.-M., T. Nakazawa, and C. H. Sui, 1991: Observations of cloud cluster hierarchies over the tropical western Pacific. *J. Geophys. Res.,* **96,** 3197–3208.

Lee, S., and I. M. Held, 1993: Baroclinic wave packets in models and observations. *J. Atmos. Sci.,* **50,** 1414–1428.

Liebmann, B., and D. L. Hartmann, 1984: An observational study of tropical–midlatitude interaction on intraseasonal timescales during winter. *J. Atmos. Sci.,* **41,** 3333–3350.

——, and C. A. Smith, 1996: Description of a complete (interpolated) OLR dataset. *Bull. Amer. Meteor. Soc.,* **77,** 1275–1277.

Livezey, R. E., and W. Y. Chen, 1983: Statistical field significance and its determination by Monte Carlo techniques. *Mon. Wea. Rev.,* **111,** 46–59.

Madden, R. A., and P. R. Julian, 1994: Observations of the 40–50 day tropical oscillation—A review. *Mon. Wea. Rev.,* **122,** 814–837.

Matthews, A. J., B. J. Hoskins, J. M. Slingo, and M. Blackburn, 1996: Development of convection along the SPCZ within a Madden–Julian Oscillation. *Quart J. Roy. Meteor. Soc.,* **122,** 669–688.

McGuirk, J. P., A. H. Thompson, and N. R. Smith, 1987: Moisture bursts over the tropical Pacific Ocean. *Mon. Wea. Rev.,* **115,** 787–798.

Meehl, G. A., G. N. Kiladis, K. M. Weickmann, M. Wheeler, D. S. Gutzler, and G. P. Compo, 1996: Modulation of equatorial subseasonal convective episodes by tropical–extratropical interaction in the Indian and Pacific Ocean regions. *J. Geophys. Res.,* **101,** 15 033–15 049.

Nakazawa, T., 1988: Tropical super clusters within intraseasonal variations over the western Pacific. *J. Meteor. Soc. Japan,* **66,** 60–75.

Salby, M. L., H. H. Hendon, K. Woodberry, and K. Tanaka, 1991: Analysis of global cloud imagery from multiple satellites. *Bull. Amer. Meteor. Soc.,* **72,** 467–480.

Slingo, J. M., 1998: Extratropical forcing of tropical convection in a northern winter simulation with the UGAMP GCM. *Quart. J. Roy. Meteor. Soc.,* **124,** 27–52.

Sui, C.-H., and K.-M. Lau, 1992: Multiscale phenomena in the tropical atmosphere over the western Pacific. *Mon. Wea. Rev.,* **120,** 407–430.

——, X. Li, K.-M. Lau, and D. Adamec, 1997: Multiscale air–sea interactions during TOGA COARE. *Mon. Wea. Rev.,* **125,** 448–462.

Takayabu, Y. N., 1994: Large-scale cloud disturbances associated with equatorial waves. Part II: Westward propagating inertio-gravity waves. *J. Meteor. Soc. Japan,* **72,** 451–465.

Ting, M., and P. D. Sardeshmukh, 1993: Factors determining the extratropical response to equatorial diabatic heating anomalies. *J. Atmos. Sci.,* **50,** 907–918.

Tomas, R. A, and P. J. Webster, 1994: Horizontal and vertical structure of cross-equatorial wave propagation. *J. Atmos. Sci.,* **51,** 1417–1430.

Webster, P. J., and J. R. Holton, 1982: Cross-equatorial response to middle-latitude forcing with a latitudinally and zonally nonuniform basic state. *J. Atmos. Sci.,* **39,** 722–733.

Weng, H., and K.-M. Lau, 1994: Wavelets, period-doubling, and time-frequency localization with application to organization of convection over the tropical western Pacific. *J. Atmos. Sci.,* **51,** 2523–2541.

Yang, G.-Y., and B. J. Hoskins, 1996: Propagation of Rossby waves of nonzero frequency. *J. Atmos. Sci.,* **53,** 2365–2378.